Stability of lithium manganese oxide ($LiMn_2O_4$) surfaces during charge/discharge processes.

Brian Ramogayana[1], Khomotso P. Maenetja[1], David Dantos-Carballal[1, 2], Nora H. de eeuw[2, 3] and Phuti E. Ngoepe[1]

[1]Materials Modelling Centre, University of Limpopo, Private Bag x1106, Sovenga, 0727, South Africa

[2]School of Chemistry, Cardiff University, Main Building, Park Place, Cardiff CF10 3AT, United Kingdom

[3]Department of Earth Sciences, Utrecht University, Budapestlaan 4, 3584 CD Utrecht, The Netherlands

E-mail: brian.ramogayana@ul.ac.za

Abstract. Surface stability and reactivity of cathode materials is one of the key aspects in improving the electrochemical performance of secondary Li-ion batteries. Lithium manganese oxide spinel attracted the most attention as a potential cathode material for lithium-ion batteries because of its three-dimensional crystal structure that allows a smooth diffusion of Li^+ in and out of the material. However, its application as a cathode material is limited by irreversible capacity fading due to manganese dissolution In the current paper, we employ the spin-polarized density functional theory calculations with on-site Coulomb interactions and long-range dispersion corrections [DFT+U−D3− (BJ)] to investigate the stability of (001), (011) and (111) surfaces during charge/discharge processes. Based on the calculated surface energies, it was observed that the Li-terminated (001) surface is the most stable with γ_r = 0.04 eV/Å^2, which is in agreement with the reported literature. To mimic charge/discharge processes, delithiated surfaces were modelled from the most stable surfaces terminations, and their stabilities were evaluated by calculating the surface free energies. As compared to the surface energies of the pure pristine facets, we observed an increase in energy during delithiation process, which indicate that the surfaces are destabilizing. However, the most stable surface upon delithiation was the (111) surface with the most dominant plane on the particle morphologies. Our work gives an insight about the surface stability and particle morphologies during charge/discharge processes.

1. Introduction

Alternative energy sources became the world's leading technology due to global warming and depleting natural resources. Although there have been many studies aimed to facilitate the movement away from the reliance on fossil fuels [1], there is still no replacement for commercially used lithium-ion batteries. Li-ion batteries are widely used because of their high-power density, long cycle life, and low self-discharge property [2]. However, recent Li-ion batteries have a limited cycling life which cannot keep up with the current advanced technologies. An improvement of the positive electrodes can facilitate the implementations of Li-ion batteries in the currently used electronic devices, electric vehicles and storage

systems. Many cathode materials such as $LiCoO_2$ [3], $LiMn_2O_4$ [4], $LiFePO_4$ [5], etc. were studied and gave an improved electrochemical performance.

Lithium manganese oxide ($LiMn_2O_4$) spinel attracted the most attention as potential cathode material because of its 3D crystal structure that allows a smooth movement of Li ions in and out of the cathode materials [6, 7]. It was considered as a suitable cathode material for Li-ion batteries because of its environmental friendliness, affordability, thermal stability, high energy density and high earth abundance of manganese [8]. However, it suffers from capacity fading due to manganese dissolution caused by the presence of the highly corrosive hydrofluoric acid continuously produced by degradation of the common $LiPF_6$-based electrolytes [9].

Various strategies were implemented to reduce Mn^{2+} dissolution into the electrolyte, which including cation doping [10, 11], replacement of commercially used electrolyte component [12] and surface coating to create an artificial barrier that limits the direct electrode-electrolyte contact [13]. Most recently, studies focused on exposing the (111) surface since it is resistant to Mn dissolution [14, 15, 16]. However, the effect of surface delithiation on the fully $LiMn_2O_4$ spinel is not completely understood. In this paper, we study the effect of delithiation on the $LiMn_2O_4$ low Miller index (001), (011) and (111) surfaces using spin-polarised density functional theory calculations. We investigate the effect of surface delithiation by calculating surface free energies of surface as we reduce the Li content and constructing their respective particle morphologies.

2. Method

The density functional theory (DFT) calculations as implemented in the Vienna Ab-initio Simulation Package (VASP) [17] was used to investigate the effect of surface delithiation on the surface stability. All calculations were carried out within the generalized gradient approximation (GGA) using the Perdew, Burke, and Ernzerhof (PBE) exchange-correlation functional [18]. We used the kinetic energy cut-off of 560 eV and the *k*-points of 5×5×5 for the integration of the reciprocal space. The projector augmented-wave (PAW) method [19] in the implemented by Kresse and Joubert [20] was used to describe the core electrons and their interaction with the valence electrons. To improve the description of the localized 3*d* electrons, we used the Hubbard correction [21] in the formulation of Dudarev *et al.* [22] and the *U* parameter was set at 4.0 eV, which was in the range of values reported in the literature [23]. We also included the semi-empirical method to model the long-range interactions [24]. We set a Gaussian smearing width of 0.05 eV to improve the convergence of the Brillion zone integrations during geometry optimizations [24].

Lithium manganese oxide ($LiMn_2O_4$) commonly known as spinel is a face-centered cubic structure with a space group *Fd*-3*m* (No. 227) and the lattice parameter of a = 8.247 Å [25]. The lithium atoms occupy the 8*a* tetrahedral sites, manganese atoms at the 16*d* octahedral sites and oxygen atoms at the 32*e* sites [26].

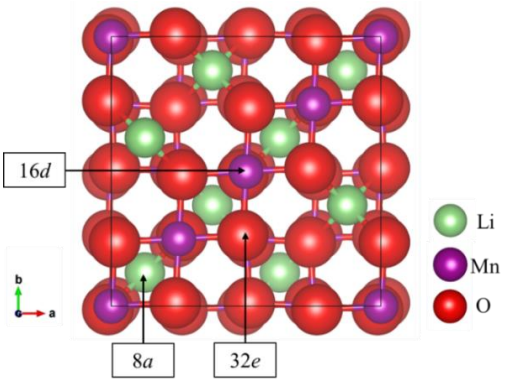

Figure 1: The crystal structure of lithium manganese oxide ($LiMn_2O_4$) spinel.

 ISBN: 978-0-620-88875-2

3. Results

3.1. Surface models

All the surfaces modelled in this study were created by cutting the fully optimised bulk using the dipole method implemented in METADISE code [27]. The resulting surfaces were represented by keeping fixed the bottom atoms at their *ab-initio* relaxed bulk positions while the rest of the atoms were allowed to relax during geometry optimization to simulate the half-relaxed slabs. The surfaces composed of the same 56 atoms (8 formula units) as in the bulk structure, with 8 Li, 16 Mn and 32 O atoms. The $LiMn_2O_4$ (001), (011) and (111) surfaces were modelled with slabs have surface areas 69.72, 48.30 and 60.38 $Å^2$, respectively.

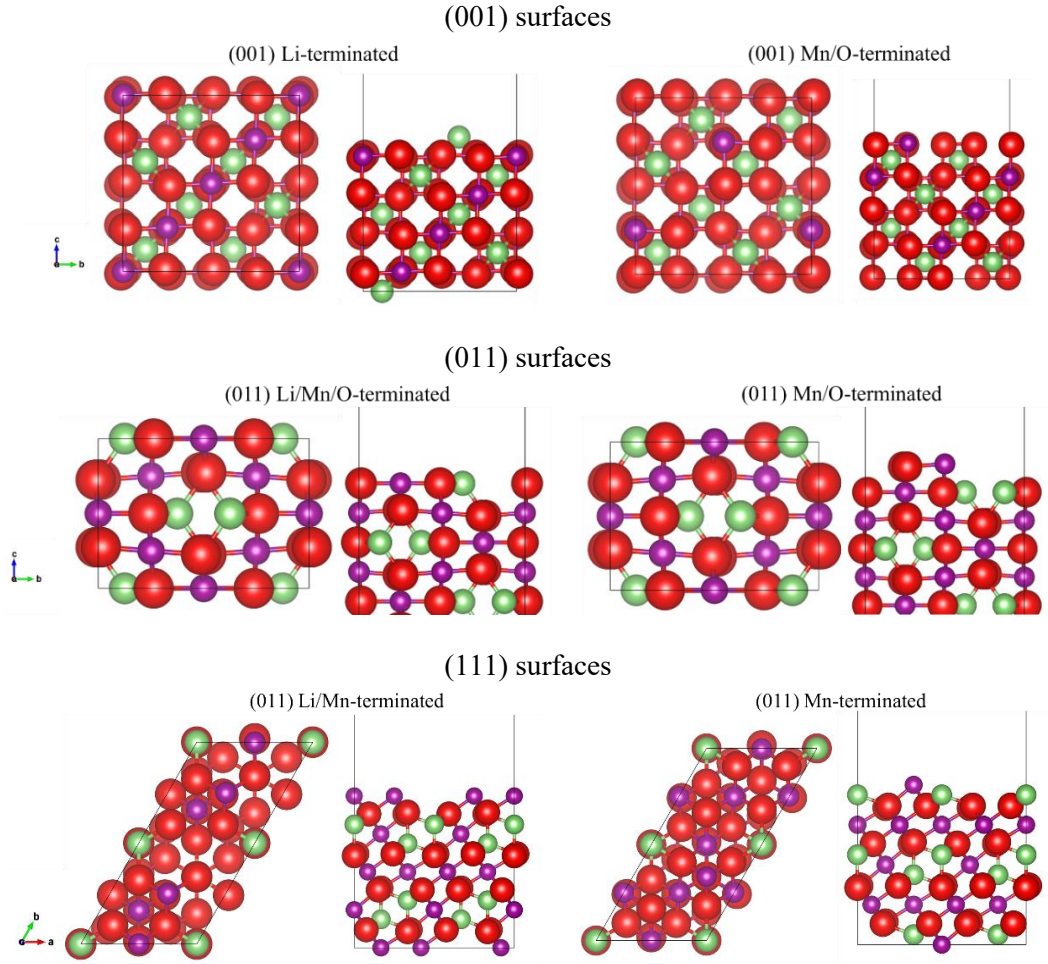

Figure 2. Top and side view of the modelled low Miller index surfaces from a fully optimized $LiMn_2O_4$ bulk structure. Crystallographic directions for the top view of (001) surface terminations is [100] for the abscissae towards the right, for the (011) surface terminations it is $[0\bar{1}1]$ for the abscissae towards the right, and for the (111) surface terminations it is $[0\bar{1}1]$ for the longest axis towards the top.

In each surface termination, a vacuum region of 15 Å was added perpendicularly to avoid interactions with the successive slabs. Various slabs, vacuum thickness and number of relaxed layers were tested until the convergence was within 1 eV per cell. In each surface orientation, we modelled two terminations which were both symmetrical and non-polar as outlined by Tasker [28]. The (001), (011) and (111) surfaces composed on two terminations, which are the Li and Mn/O-terminated slabs for

(001), Li/Mn/O and Mn/O-terminated for (011), and Li/Mn and Mn-terminated slabs for (111) surfaces (see Figure 2).

3.2. Surface energies

Energy minimization of (001), (011) and (111) surfaces were carried out to obtain their respective surface energies. We determined the surface energies for the unrelaxed surface from a single point calculations of the slabs before relaxation. The unrelaxed surfaces energies (γ_u) were calculated as:

$$\gamma_{\mathrm{u}} = \frac{E_{\mathrm{u}} - E_{\mathrm{b}}}{2A} \quad (1)$$

where E_{u} is the total energy of unrelaxed facet, E_{b} is the energy of the fully optimized bulk with the same number of formula units as in the slabs and A is the surface area of each slab. During surface relaxation, the uppermost atoms were allowed to relax and the bottom atoms were kept fixed at bulk positions. The relaxed surface energies (γ_r) for these half-relaxed slabs were calculated using:

$$\gamma_r = \frac{E_{\mathrm{r}} - E_{\mathrm{b}}}{A} - \gamma_{\mathrm{u}} \quad (2)$$

where E_{r} is the energy of half relaxed surface. The degree of relaxation (R) was also calculated for all the surfaces as:

$$R = \frac{\gamma_{\mathrm{u}} - \gamma_{\mathrm{r}}}{\gamma_{\mathrm{u}}} \times 100 \quad (3)$$

Table I. Surface energies of the low Miller index surface for the relaxed (γ_r) and unrelaxed (γ_u) slab.

Surface	Termination	γ_u (eV/Å^2)	γ_r (eV/Å^2)	R (%)
(001)	Li	0.07	0.04	43.7
	Mn/O	0.15	0.11	28.7
(011)	Li/Mn/O	0.10	0.05	50.0
	Mn/O	0.10	0.07	37.2
(111)	Li/Mn	0.08	0.05	38.0
	Mn	0.21	0.09	57.9

Table 1 summarizes the surface energies (for both unrelaxed and relaxed slabs) and the degree relaxation for the modelled surface shown in Figure 2. Considering the most stable surface as the one with the lowest surface energy, the (001) surface is observed as the most stable in both relaxed and unrelaxed slabs. The calculated surface energies indicated that the Li-terminated (001) surface has the lowest surface energy of γ_r = 0.04 eV/Å^2 compared to other facets. With reference to the reported literature, the calculated surface energy for the Li-terminated (001) facet was in the range between 0.26-0.96 J/m^2 (0.02 and 0.06 eV/Å^2) [29]. Surface energies of both the relaxed and unrelaxed slabs show an increasing trend for the most stable termination, {(001) < (011) < (111)}, and therefore a decreasing surface stability. The most stable surface terminations for (001), (011) and (111) facets are the Li, Li/Mn/O and Li/Mn-terminated slabs, respectively. The relaxation percentages indicate that the (111) Mn–terminated (111) surface had the highest geometry relaxation while the Mn/O-terminated (001) had the lowest geometry relaxation percentage.

3.3. Surface free energies

To mimic the Li intercalation during charge/discharge processes, we modelled the partially delithiated surfaces by removing the Li atoms from the uppermost atomic layer of the most stable surface terminations. The delithiated surfaces were modelled by removing only the Li atoms from the atomic layers which were allowed to move during geometry optimization. The stability of the modelled

delithiated surfaces were investigated by calculating surface energies for different Li concentrations using equation:

$$\sigma = \gamma_{\mathrm{r}} + \frac{E_{\mathrm{d}} - E_{\mathrm{r}} + (8 - N_{\mathrm{Li}})E_{\mathrm{Li}}}{A} \quad (3)$$

where E_{d} is the energy of the delithiated slab, E_{r} is the energy of the pristine slab, $8-N_{\mathrm{Li}}$ is the number of lithium atoms removed from the slab and E_{Li} is the energy of one atom in the bulk of the body-centered cubic (*bcc*) lithium. Table II summarize the surface free energies (σ) for slabs with different Li concentration. Note that when there are no surface modifications (such as surface doping, adsorption or delithiation), the surface energies and the surface free energies have the same magnitude [30]. In every surface orientation, we modelled slabs with compositions $Li_8Mn_{16}O_{32}$, $Li_7Mn_{16}O_{32}$ and $Li_6Mn_{16}O_{32}$. Generally, we observe an increase in surface free energies upon delithiation compared to the surface energy for the fully lithiated surfaces, indicating surface destabilizing effect. After removing a single Li atom (x = 0.125), we observe that the (001) surface destabilises but still remain the most stable surface with σ = 0.12 eV/ Å^2, followed by the (111) facet with σ = 0.14 eV/ Å^2 and then (001) surface with the highest surface free energy of σ = 0.31 eV/ Å^2. Upon the removal of two Li atoms (x = 0.250), the lowest surface free energy was the (111) facet with σ = 0.09 eV/Å^2, while the slab with the highest surface free energy was the (001) facet with σ = 0.10 eV/Å^2.

Table II. Surface free energies (σ) for the partially delithiated surfaces at different Li content, showing the surface compositions and the number of Li atoms removed (x). Note that for x = 0, the surface free energy is equivalent to the surface energy ($\sigma = \gamma$).

Surface	Composition	x	σ (eV/ Å^2)
(001)	$Li_8Mn_{16}O_{32}$	0	0.04
	$Li_7Mn_{16}O_{32}$	0.125	0.12
	$Li_6Mn_{16}O_{32}$	0.250	0.10
(011)	$Li_8Mn_{16}O_{32}$	0	0.05
	$Li_7Mn_{16}O_{32}$	0.125	0.31
	$Li_6Mn_{16}O_{32}$	0.250	0.14
(111)	$Li_8Mn_{16}O_{32}$	0	0.05
	$Li_7Mn_{16}O_{32}$	0.125	0.14
	$Li_6Mn_{16}O_{32}$	0.250	0.09

3.4. Particle morphologies

The Wulff construction for particle morphologies was based on the famous paper on the heterogeneous substances by J.W. Gibbs [31]. Figure 3 summarizes the constructed particle morphology for the fully lithiated and partially delithiated surfaces. The particle morphologies were constructed from the surface free energies of respective Li concentrations. The fully lithiated particle morphologies are dominated by the (001) Li terminated surface, which is similar to the octahedron-shaped observed in literature [25]. Upon delithiation, the morphology clearly indicates that as we reduce the Li content, the (001) surface plane decreases, while the (111) plane becomes the most dominant facet. The (011) surface turn to disappear in the Wulff morphology upon delithiation because of its higher surface free energy with respect to the (001) and (111) planes.

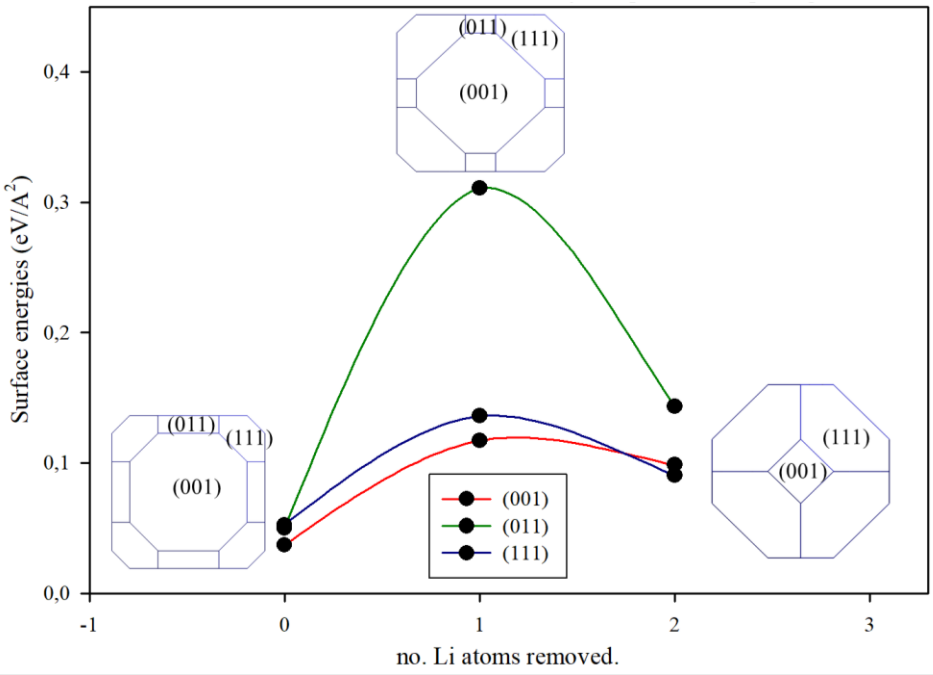

Figure 3. The effect of delithiation onto the $LiMn_2O_4$ spinel surfaces at different Li content. This was investigated by calculating the surface free energies of partially delithiated surfaces at various Li concentrations and contracting their respective particle morphologies.

4. Conclusion

Using the density functional theory calculations, we successfully investigated the effect of delithiation on the three low Miller index (001), (011) and (111) Surfaces. We modelled the fully lithiated and partially delithiated surfaces from an optimised bulk and the most stable surface terminations, respectively. The calculated surface energies show that Li-terminated (001) facet is the most stable surface with γ_r = 0.04 eV/Å^2, which is in agreement with the reported literature. To mimic the charge/discharge surfaces, we modelled the delithiated surfaces from the most stable termination by removing the Li atoms from the uppermost atomic layers. The surface free energies (σ) calculated for the modelled partially delithiated surface were higher as compared to the surface energies of the fully lithiated facets, which indicated that the surfaces were destabilising as the Li content decreases. Furthermore, we observed a decrease in (001) plane on the particle morphologies, while (111) surface become the most dominant slab upon delithiation.

Acknowledgement

This work was performed using the computational facilities of the Advanced Research Computing @ Cardiff (ARCCA) Division, Cardiff University. We acknowledge the South African Research Chair Initiative of the Department of Science and Technology, the National Research Foundation in Pretoria and the Centre for High-Performance Computing in Cape Town. Part of the study was undertaken using the Supercomputing Facilities at Cardiff University operated by ARCCA on behalf of the HPC Wales and Supercomputing Wales (SCW) projects. The authors also wish to thank the collaboration between the Material Modelling Centre (MMC), University of Limpopo and Advanced Research Computing @ Cardiff (ARCCA) Division, Cardiff University.

5. References

[1] S.k. Nandi and H.R. Ghosh 2010 *Energy* **35** 3040.

[2] S. Goriparti, E. Miele, F. De Angelis, E. Di Fabrizio, R.P. Zaccaria and C. Capiglia 2014 *J. Power sources* **257** 421.

[3] P. Byeon, H.B. Bae, H.S. Chung, S.G. Lee, J.G. Kim, H.J. Lee, J.W. Choi and S.Y. Chung 2018 *Adv. Funct.l Mater.* **28** 1804564.

[4] C.Y. Ouyang, S.Q. Shi, Z.X. Wang, H. Li, X.J Huang and L.Q. Chen 2004 *Europhy. Lett.* **67** 28.

[5] T. Mueller, G. Hautier, A. Jain and G. Ceder 2011 *Chem. Mater.* **23** 3854.

[6] J. Kim and A. Marnthiram 1997 *Nature* **390** 265.

[7] S.T. Lee, K. Raveendranath, R.M. Tomy, N.A. George, S. Jayalekshmi and J. Ravi 2007 *J. Phys. D: Appl. Phys.* **40** 3807.

[8] K.R. Ragavendran, H. Xia, G. Yang, D. Vasudevan, B. Emmanuel, D. Sherwood and A.K. Arof 2014 *PCCP* **16** 2553.

[9] M. Wohlfahrt-Mehrens, C. Vogler and J. Garche 2004 *J. Power sources* **127** 58.

[10] M. Michalska, D.A. Ziółkowska, J.B. Jasiński, P.-H. Lee, P. Ławniczak, B. Andrzejewski, A. Ostrowski, W. Bednarski, S.H. Wu and J.Y. Lin 2018 *Electrochim. Acta* **276** 37.

[11] A. M. Kannan and A. Manthiram 2002 *Electrochem. Solid-State Lett.* **5** 167.

[12] G. Xu, Z. Liu, C. Zhang, G. Cui and L. Chen 2015 *J. Mater. Chem. A* **3** 4092.

[13] D. Guan, J.A. Jeevarajan and Y. Wang 2011 *Nanoscale* **3** 1465.

[14] C.J. Jafta, F. Nkosi, L. le Roux, M.K. Mathe, M. Kebede, K. Makgopa, Y. Song, D. Tong, M. Oyama, N. Manyala and S. Chen 2013 *Electrochim. Acta* **110** 228.

[15] F.P. Nkosi, C.J. Jafta, M. Kebede, L. Le Roux, M.K. Mathe and K.I. Ozoemena 2015 *RSC Adv.* **5** 32256.

[16] Y. Xiao, X.D. Zhang, Y.F. Zhu, P.F. Wang, Y.X. Yin, X. Yang, J.L. Shi, J. Liu, H. Li, X.D. Guo and B.H. Zhong 2019 *Adv. Sci.* **6** 1801908.

[17] G. Kresse and J. Furthmüller 1996 *Phys. Rev. B* **54** 11169.

[18] J.P. Perdew, K. Burke and M. Ernzerhof 1996 *Phys. Rev. lett.* **77** 11169.

[19] P.E. Blöchl 1994 *Phys. Rev. B* **50** 17953.

[20] G. Kresse and D. Joubert 1999 *Phys. Rev. B* **19** 1758.

[21] V.I. Anisimov, M.A. Korotin, J. Zaanen and O.K. Andersen 1992 *Phys. Rev. lett.* **68** 345.

[22] S.L. Dudarev, G.A Botton, S.Y. Savrasov, C.J. Humphreys and A.P. Sutton 1998 *Phys. Rev. B* **57** 1505.

[23] D. Santos-Carballal, P.E. Ngoepe and N.H. de Leeuw 2018 *Phys. Rev. B* **97** 085126.

[24] S. Grimme, J. Antony, S. Ehrlich and H. Krieg 2010 *J. Chem. Phys.* **132** 154104.

[25] J.S. Kim, K. Kim, W. Cho, W. H. Shin, R. Kanno and J. W.Choi 2012 *Nano lett.* **12** 6358.

[26] S. K. Mishra and G. Ceder 1999 *Phys. Rev. B* **59** 6120.

[27] G. W. Watson, E. T. Kelsey, N. H. de Leeuw, D. J. Harris and S. C. Parker 1996 *J. Chem. Soc. Faraday Trans.* **92** 433.

[28] P.W. Tasker 1979 *J. Phys. C: Solid State Phys.* **12** 4977.

[29] A. Karim, S. Fosse, and K. A. Persson 2013 *Phys. Rev. B* **87** 075322.

[30] V. Postica, A. Vahl, J. Strobel, D. Santos-Carballal, O. Lupan, A. Cadi-Essadek, N.H. de Leeuw, F. chütt, O. Polonskyi, T. Strunskus and M. Baum 2018 *J. Mater. Chem. A* **6** 23669.

[31] J.W. Gibbs 1875 *Trans. Conn. Acad. Arts Sci.* **3** 108.